Electronic Supplementary Material (ESI) for Journal of Materials Chemistry A.

Supporting information for:

Zinc-Based Spinel Cathode Materials for Magnesium Rechargeable Batteries: Toward Reversible Spinel–Rocksalt Transition

Kohei Shimokawa,* Taruto Atsumi, Maho Harada, Robyn E. Ward, Masanobu Nakayama, Yu Kumagai, Fumiyasu Oba, Norihiko L. Okamoto, Kiyoshi Kanamura, and Tetsu Ichitsubo*

E-mail: shimokawa.kohei@imr.tohoku.ac.jp; tichi@imr.tohoku.ac.jp

*To whom correspondence should be addressed

Supporting Section S1: Cation Arrangement in Stoichiometric $MgCo_2O_4$ and $ZnCo_2O_4$

Table S1: Comparison of spinel structure parameters (space group, $Fd\bar{3}m$) between GA-derived computational and reported experimental results for $MgCo_2O_4$. Oxygen parameter refers to the fractional coordinates of x (= y = z) at 32e sites.

$MgCo_2O_4$	Computational	Experimental[S1]
Cubic lattice parameter, a	8.0664	8.1074(1)
Site occupancy of Co at 8a	0	0.475(2)
Oxygen parameter, u	0.389	0.3864(1)

Table S2: Comparison of spinel structure parameters (space group, $Fd\bar{3}m$) between GA-derived computational and reported experimental results for $ZnCo_2O_4$. Oxygen parameter refers to the fractional coordinates of x (= y = z) at 32e sites.

$ZnCo_2O_4$	Computational	Experimental[S2]
Cubic lattice parameter, a	8.0481	8.1019(7)
Site occupancy of Co at 8a	0	0.20(1)
Oxygen parameter, u	0.389	0.3881(1)

Details of Monte Carlo Simulation

To quantitatively evaluate the cation configuration at elevated temperatures, DFT derived Monte Carlo simulation with cluster expansion technique was used. Firstly, total electron energies for 50 symmetrically distinct configurations each of $MgCo_2O_4$ and $ZnCo_2O_4$ were calculated using the DFT + U approach. Subsequently, a subset of the calculated configurations with total energies corresponding to different Mg/Co and Zn/Co arrangements within each ccp oxide ion array was converted to effective cluster interactions (ECI) to estimate the total energy of the crystal with each arbitrary cation arrangement rapidly and precisely. This can be done using a generalized lattice model based on the cluster expansion formal-

ism.[S3,S4] The total energies of various cation configurations calculated using DFT (EDFT, horizontal axis) vs the cluster expansion formalism fitted ECI values (EECI, vertical axis), give good accordance between DFT- and ECI- derived total energies (Fig. S1). Canonical MC calculations using fitted ECI values were performed using a spinel supercell with 7560 cation sites in the temperature range 300–2100 K with several temperature cycles (Fig. 2a in the main text).

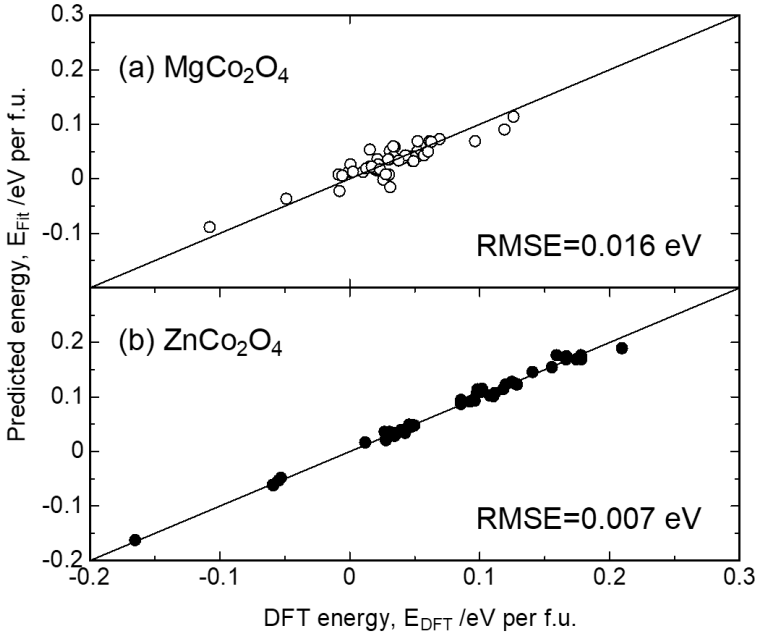

Figure S1: Diagnostic plots of fitted energies (predicted energy), E_{Fit}, based on cluster expansion formalism against DFT energy, E_{DFT}.

Supporting Section S2: Migration Energies of Divalent Cations in Spinel-Type $MgCo_2O_4$ and $ZnCo_2O_4$

Fig. 2b in the main text presents the energy profile of Mg^{2+} or Zn^{2+} ion hopping, respectively, obtained by the NEB methods in $Mg_7Co_{16}O_{32}$ and $Zn_7Co_{16}O_{32}$ with normal spinel structure where one of the Mg sites is vacancy. (For convenience purposes, we refer these vacant compounds, hereinafter, as $MgCo_2O_4$ and $ZnCo_2O_4$, unless mentioned specially). As mentioned in the main text, the migration energy is 452 meV and 612 meV for the Mg^{2+} and Zn^{2+} jump, respectively. The diffusion coefficient, D, for ion migration in solids can be expressed as below,[S5]

$$D = a^2 \nu^* exp \frac{-E_m}{k_B T} \tag{1}$$

where a is the jump path distance, ν is the attempt frequency, E_m is the migration energy, T is the temperature in Kelvin and k_B is the Boltzmann constant. The diffusion distance or root mean square displacement, L, can be described from random walk theory using diffusion coefficient D and time, t, as below,

$$L = \sqrt{2dDt} \tag{2}$$

where d is dimension of migration path ($d = 3$ for the spinel compounds). Table S3 lists the estimated diffusion coefficients at room temperature over a 1-hour diffusion distance, i.e. root mean square displacement, of Mg and Zn ions by assuming attempt frequency of 1012 Hz from literature.[S5] The results indicate that divalent cation diffusion is kinetically possible at a rate of 1C and even at room temperature via nano-scaled particles synthesis.

Table S3: Estimated diffusion coefficients, D, and diffusion distances, L, by DFT-NEB results (Figure 2b) and eqn. 1–2 for $MgCo_2O_4$ and $ZnCo_2O_4$ with normal spinel structure.

Material	$D\ /cm^2\ s^{-1}$	$L\ /nm\ h^{-1}$
$MgCo_2O_4$	2.9×10^{-11}	7900
$ZnCo_2O_4$	5.5×10^{-14}	340

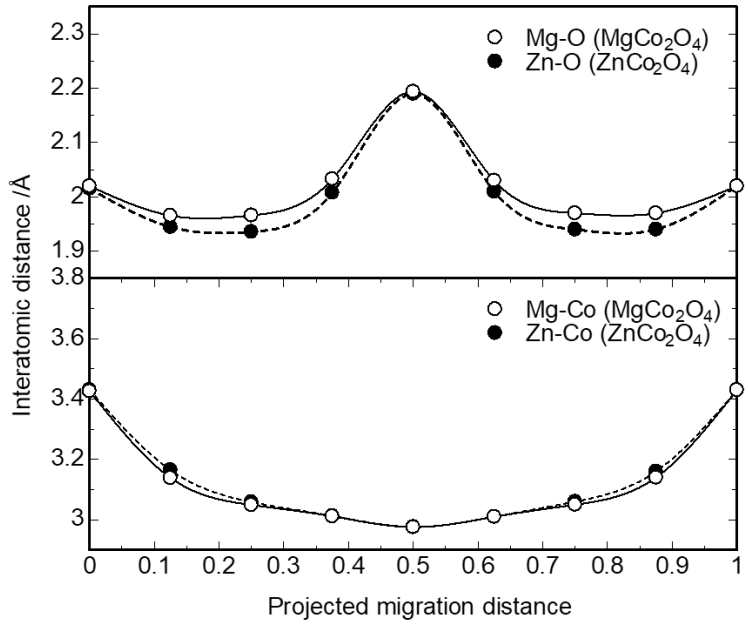

Figure S2: Variation of interatomic distance between hopping divalent cations, Mg^{2+} or Zn^{2+}, and oxide ions (upper panel) or Co ions (lower panel) for $MgCo_2O_4$ or $ZnCo_2O_4$, respectively.

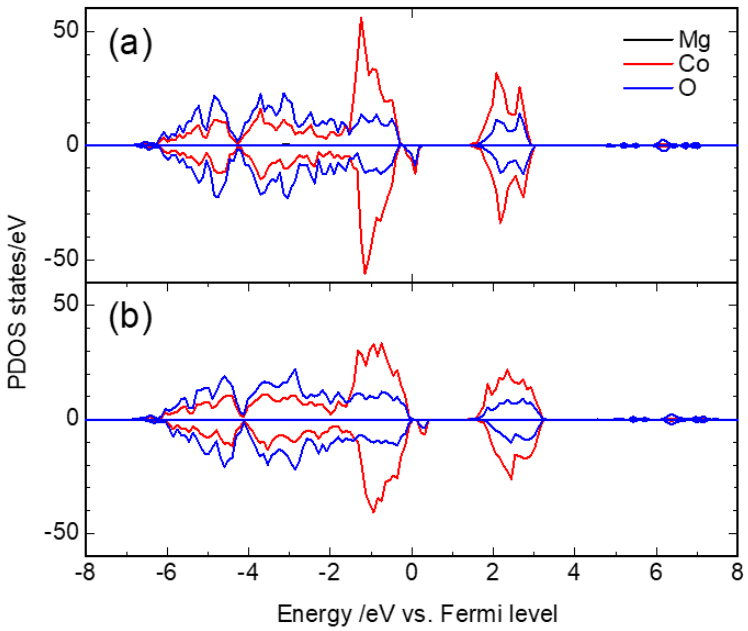

Figure S3: Partial density of states (PDOS) for $MgCo_2O_4$. The PDOS in panels (a) and (b) are of the electronic structures for a hopping Mg at a tetrahedral 8a and octahedral 16c site in $MgCo_2O_4$, respectively. The energy drop at 16c sites in $MgCo_2O_4$ can be ascribed to the larger polyhedral volume at octahedral 16c sites compared to the tetrahedral 8a sites, which cause smaller short-range repulsive interaction arising from electron cloud overlapping.

Supporting Section S3: Influence of Mechanical Strain on Electrode Materials[S6]

The reactions in the magnesium rechargeable batteries utilizing spinel-to-rocksalt transition materials as the cathode are as follows:

$$\text{Anode: } Mg = Mg^{2+} + 2e$$
$$\text{Cathode: } AB_2O_4(spinel) + Mg^{2+} + 2e = MgAB_2O_4(rocksalt)$$
$$\text{Total: } AB_2O_4(spinel) + Mg = MgAB_2O_4(rocksalt)$$

If the reactions are assumed to occur without any strain, *emf* vs. Mg^{2+}/Mg is expressed as

$$emf = -\frac{\mu_{rocksalt} - \mu_{spinel} - \mu_{Mg}}{2F} = -\frac{\Delta G_{chem}}{2F} \tag{3}$$

where F is the Faraday constant. When the spinel phase stores the strain energy U_S (per 1 mole of AB_2O_4), *emf* vs. Mg^{2+}/Mg is given by

$$emf = -\frac{\Delta G_{chem} + U_S}{2F} \tag{4}$$

$$U_S = BV_m\frac{\Delta V}{V} \tag{5}$$

where B is the bulk modulus, V_m is the molar volume, and $\frac{\Delta V}{V}$ is the volume change modulus. The bulk modulus of Co-based spinel oxides is estimated to be about 160 GPa by ab initio calculation. V_m of $ZnCo_2O_4$ is approximately $4\times10^{-5}\ m^3/mol$. If the volume change modulus is assumed as 0.08 that is half of the volume change between the observed spinel and rocksalt phases, U_S is calculated to be 20 kJ/mol. Therefore, the potential drop due to the strain energy $-\frac{U_S}{2F}$ amounts to ~ -0.1 V.

Supporting Section S4: Additional Experimental Results and Analysis

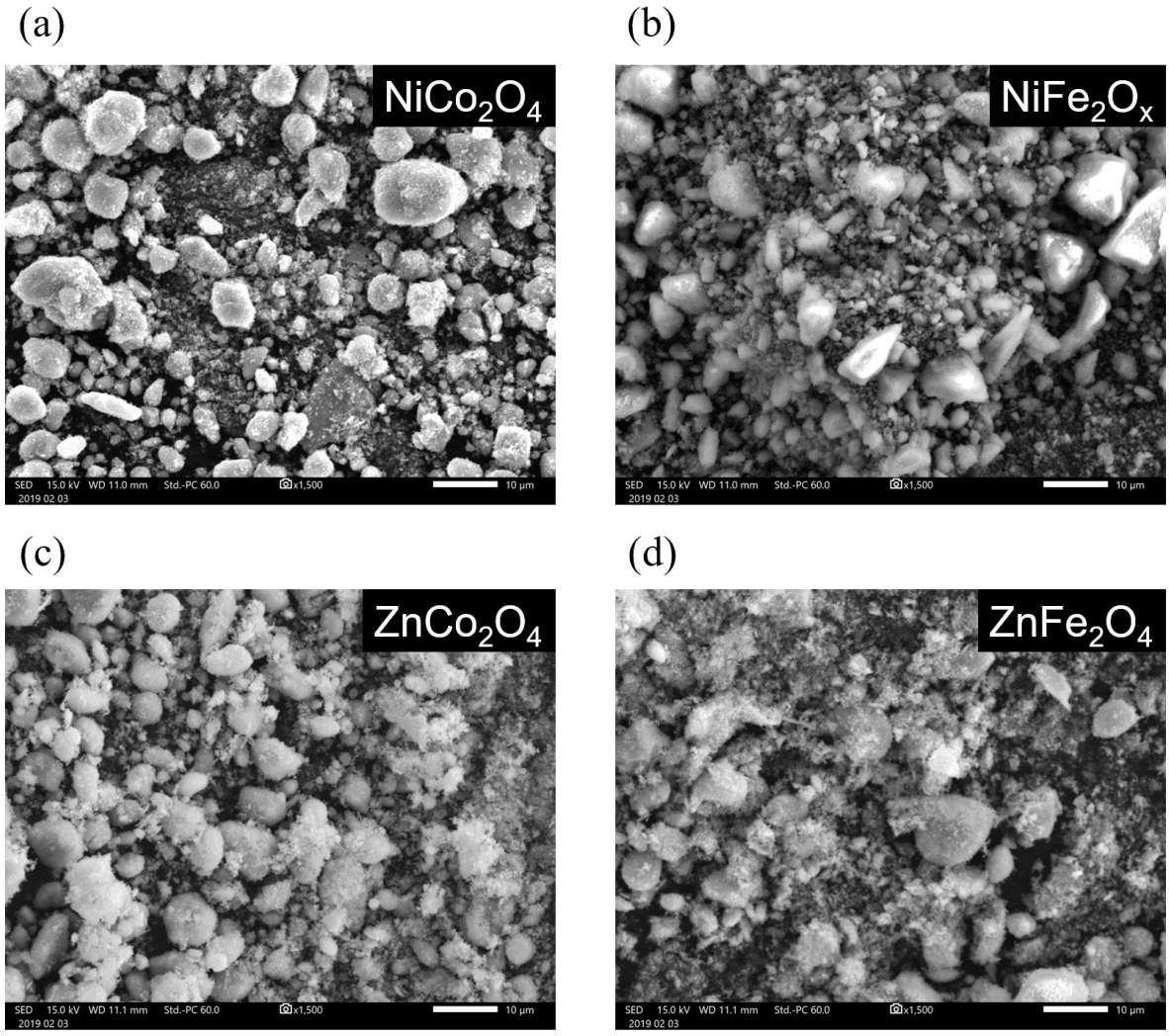

Figure S4: SEM images of the synthesized powder of (a) $NiCo_2O_4$, (b) $NiFe_2O_4$, (c) $ZnCo_2O_4$, and (d) $ZnFe_2O_4$ after calcination at 350 °C. The secondary particle size was 1–10 μm due to the aggregation for each composition.

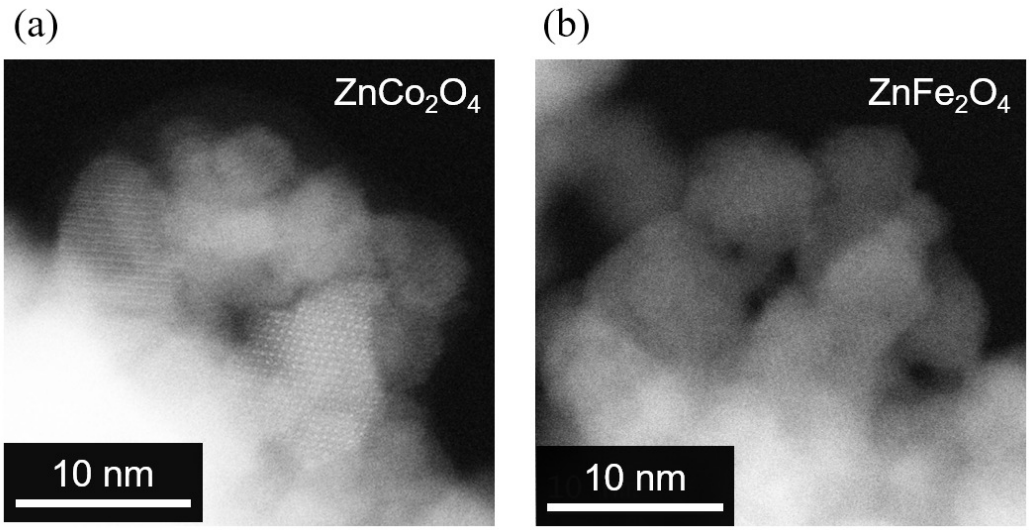

Figure S5: HAADF-STEM image of (a) $ZnCo_2O_4$ after calcination at 350 °C and (b) $ZnFe_2O_4$ without calcination, whose primary particle size of each compound was ∼10 nm .

Table S4: Details of the solutions prepared for the synthesis of the spinel oxides by the inverse coprecipitation method.[S1] The solution A, metallic nitrate salts aqueous solution, is added dropwise into the solution B, the sodium carbonate precipitation solution, to obtain the precursor for each spinel oxide.

Spinel oxides	Solution A	Solution B
$ZnFe_2O_4$	0.08 M $Zn(NO_3)_2{\cdot}6H_2O$ 0.16 M $Fe(NO_3)_3{\cdot}9H_2O$	0.35 M Na_2CO_3
$NiFe_2O_4$	0.08 M $Ni(NO_3)_2{\cdot}6H_2O$ 0.16 M $Fe(NO_3)_3{\cdot}9H_2O$	0.35 M Na_2CO_3
$ZnCo_2O_4$	0.08 M $Zn(NO_3)_2{\cdot}6H_2O$ 0.16 M $Co(NO_3)_2{\cdot}6H_2O$	0.35 M Na_2CO_3
$NiCo_2O_4$	0.08 M $Ni(NO_3)_2{\cdot}6H_2O$ 0.16 M $Co(NO_3)_2{\cdot}6H_2O$	0.35 M Na_2CO_3

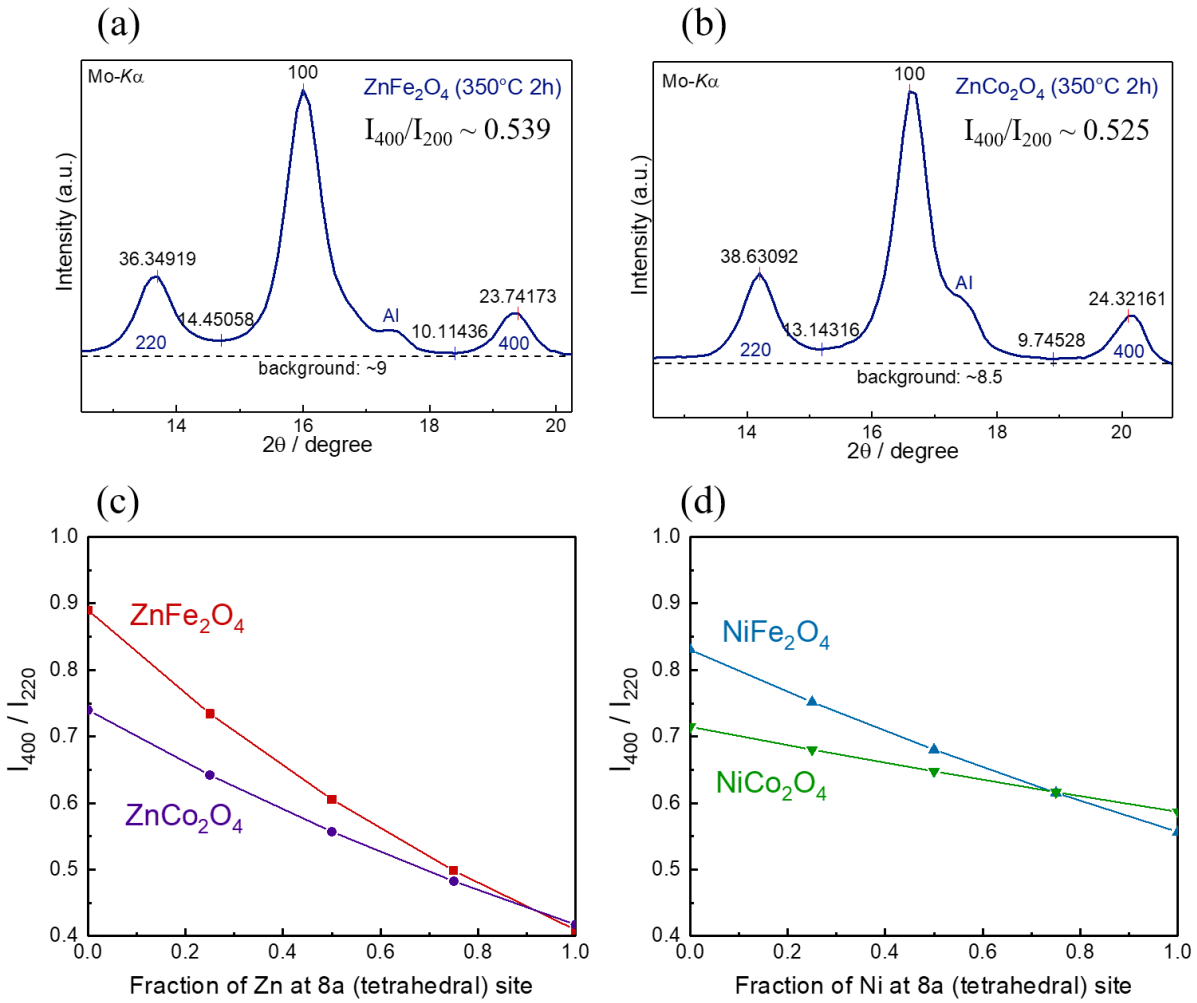

Figure S6: Obtained XRD profiles of (a) $ZnFe_2O_4$ and (b) $ZnCo_2O_4$, and the values of I_{400}/I_{220} depending on the fraction of Zn at tetrahedral 8a sites in the spinel structure determined by simulation for the (c) Zn-based and (d) Ni-based spinel oxides. The intensity ratios of I_{400}/I_{220} estimated from the experimental results are within 0.50–0.55 for both $ZnFe_2O_4$ and $ZnCo_2O_4$. This suggests that most of Zn^{2+} ions occupy tetrahedral 8a sites in the obtained spinel oxides. In the case of $NiCo_2O_4$, the obtained XRD profile shows the intensity ratio of $I_{400}/I_{220} > 1$ (Figure 3 in the main text), but such a value is not reproduced in simulation, which indicates that the obtained $NiCo_2O_4$ contains some rocksalt-like defects.

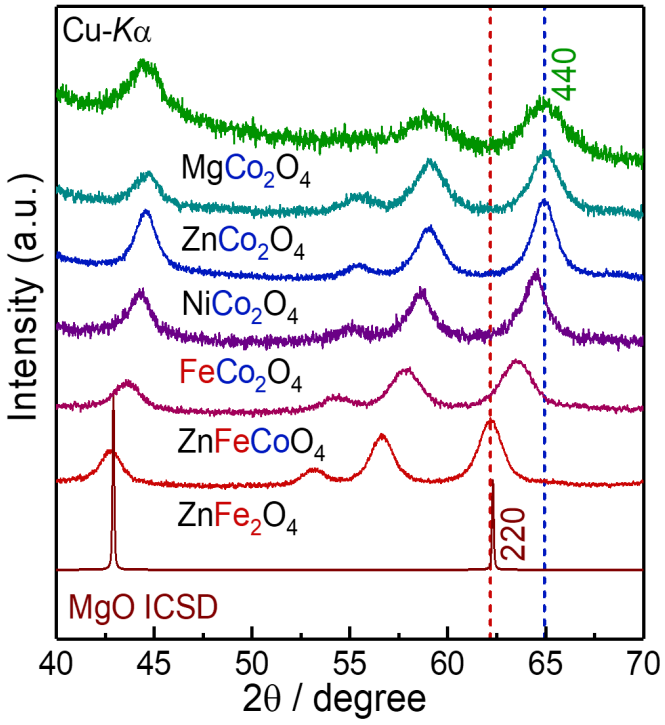

Figure S7: XRD profiles of the obtained spinel oxides containing Co and/or Fe. The lattice constant systematically varies depending on the molar ratio of Fe/Co. Although Co-based spinel oxides have much smaller lattice size compared to that of rocksalt MgO, the lattice size is expanded by the replacement of Co by Fe. Especially, the lattice size of $ZnFe_2O_4$ is comparable with that of MgO.

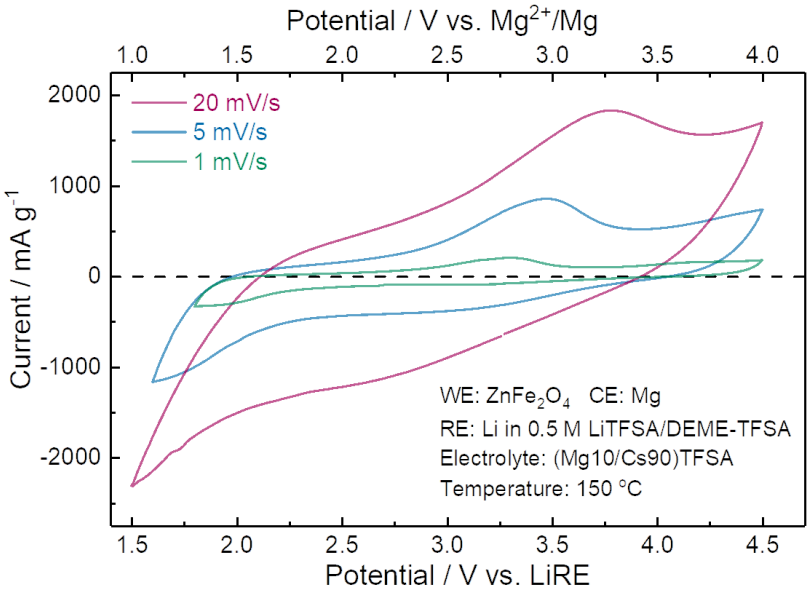

Figure S8: Cyclic voltammograms of $ZnFe_2O_4$ in (Mg10/Cs90)TFSA electrolyte at 150 °C with the scan rates of 1 mV s^{-1}, 5 mV s^{-1}, and 20 mV s^{-1}.

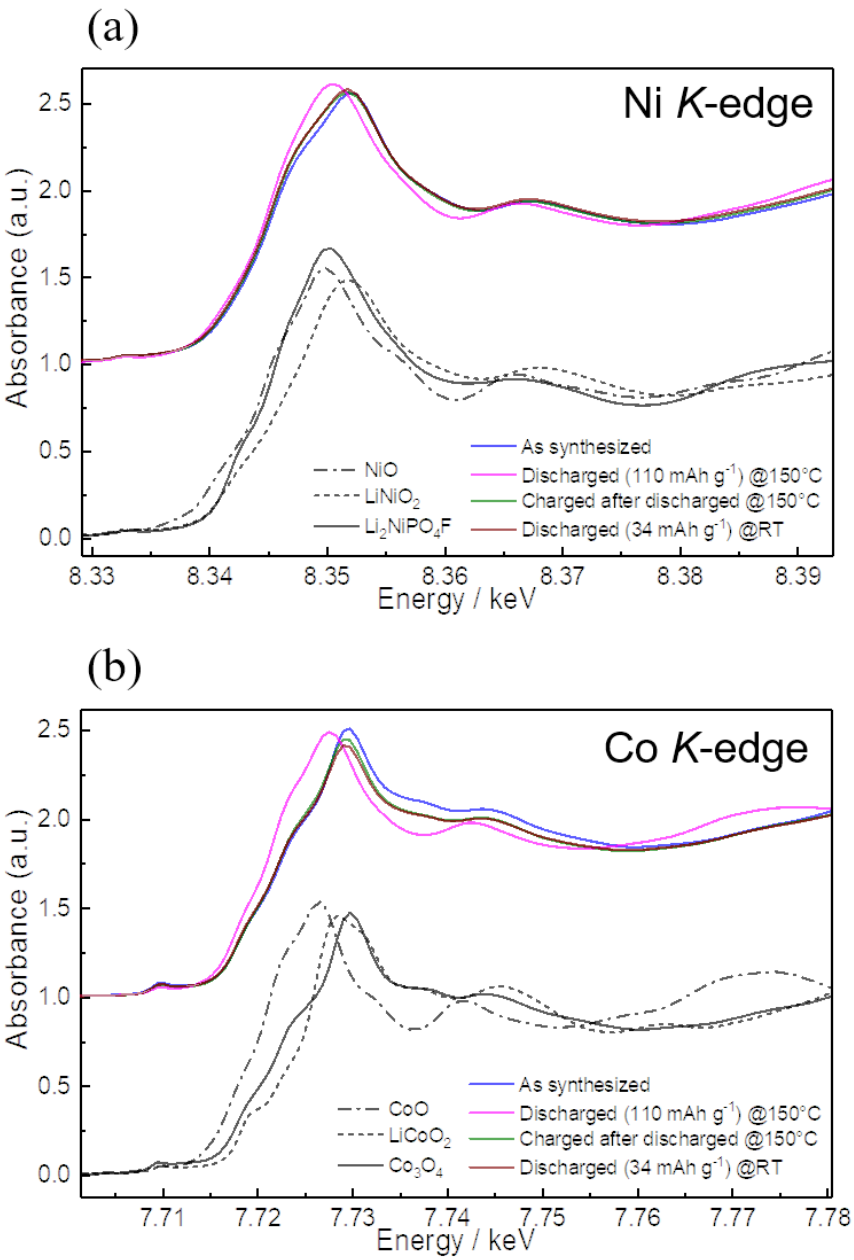

Figure S9: XANES spectra measured for $NiCo_2O_4$ after discharge/charge around (a) Ni *K*-edge and (b) Co *K*-edge using synchrotron radiation. Two kinds of discharged samples were prepared by holding 2.2 V vs. Li^+/Li for 8 hours in (Mg10/Cs90)TFSA at 150 °C (110 mAh g^{-1}), and by holding 2.2 V vs. Li^+/Li for 12 hours in 0.5 M $Mg(TFSA)_2$/G3 at room temperature (34 mAh g^{-1}). A charged sample was prepared by holding 4.5 V vs. Li^+/Li for 3 hours after the discharge (holding 2.2 V vs. Li^+/Li for 8 hours) in (Mg10/Cs90)TFSA at 150 °C. The XANES profiles around Co *K*-edge suggest that the valence change of Co^{2+}/Co^{3+} occurs with discharge/charge, whereas the shift of the profiles around Ni *K*-edge was not clearly observed.

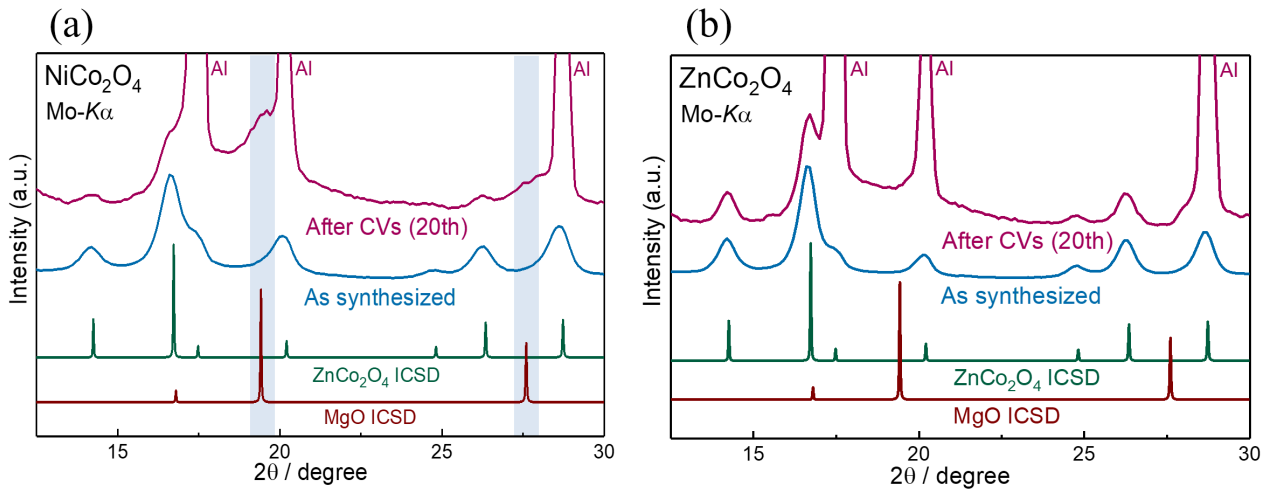

Figure S10: XRD profiles measured for the electrodes after CVs for (a) $NiCo_2O_4$ and (b) $ZnCo_2O_4$. The CV measurements were stopped at charged state (ideally with spinel phase), however, the profile of $NiCo_2O_4$ shows that there remains substantial amount of rocksalt phase whose lattice constant is similar to that of MgO. This suggests that the observed degradation of $NiCo_2O_4$ is due to the formation of such the irreversible rocksalt phase.

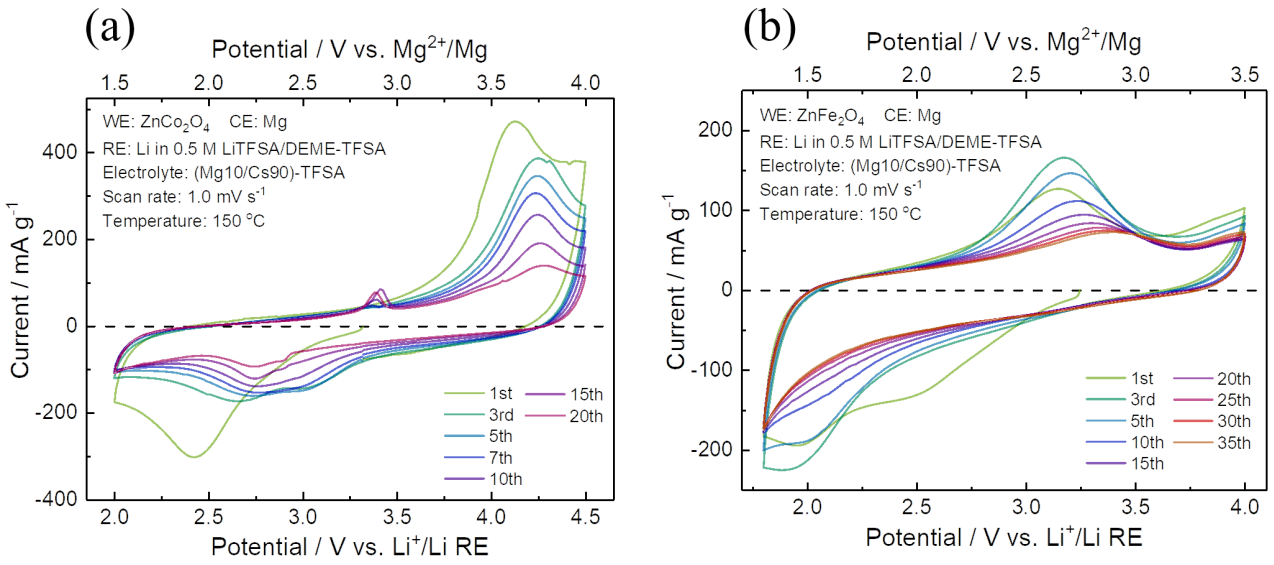

Figure S11: Cyclic voltammograms showing the evolution of electrochemical performance with long-term cycling measured for (a) $ZnCo_2O_4$ and (b) $ZnFe_2O_4$ in (Mg10/Cs90)TFSA electrolyte at 150 °C.

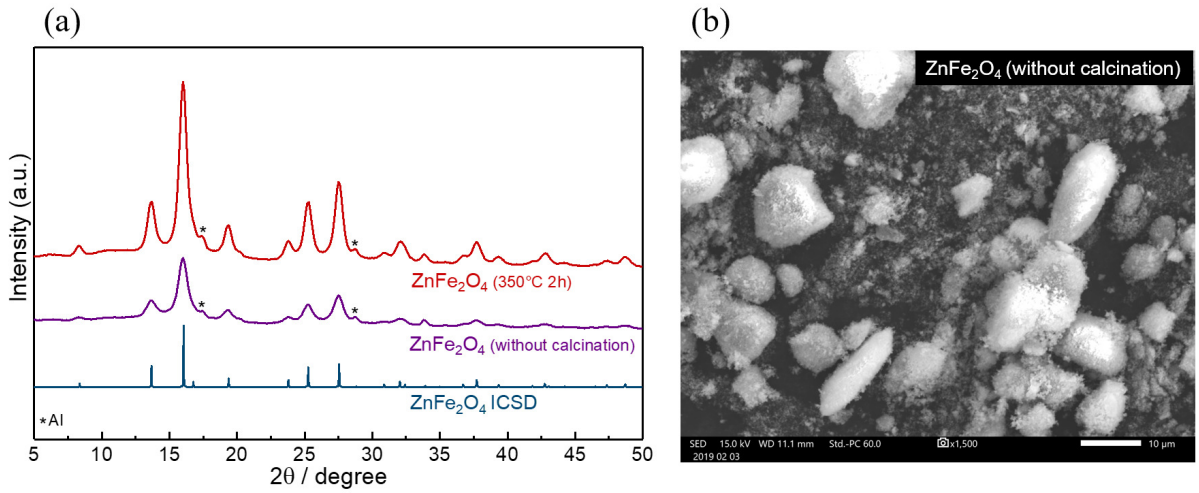

Figure S12: (a) XRD profiles of the $ZnFe_2O_4$ obtained by the inverse coprecipitation method.[S1] The profile of the sample without calcination shows relatively broad peaks corresponding to those of spinel $ZnFe_2O_4$, which indicates that nanocrystalline spinel $ZnFe_2O_4$ was successfully synthesized without calcination. (b) SEM image of $ZnFe_2O_4$ without calcination, whose secondary particle size was 1–10 μm.

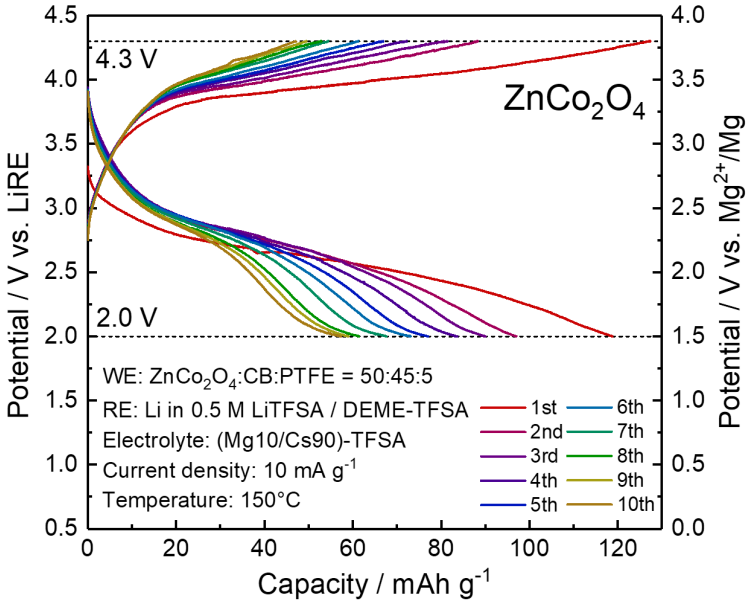

Figure S13: Discharge/charge performance of $ZnCo_2O_4$ with a comparable amount of carbon black and PTFE binder ($ZnCo_2O_4$:carbon:PTFE = 50:45:5) at 150 °C.

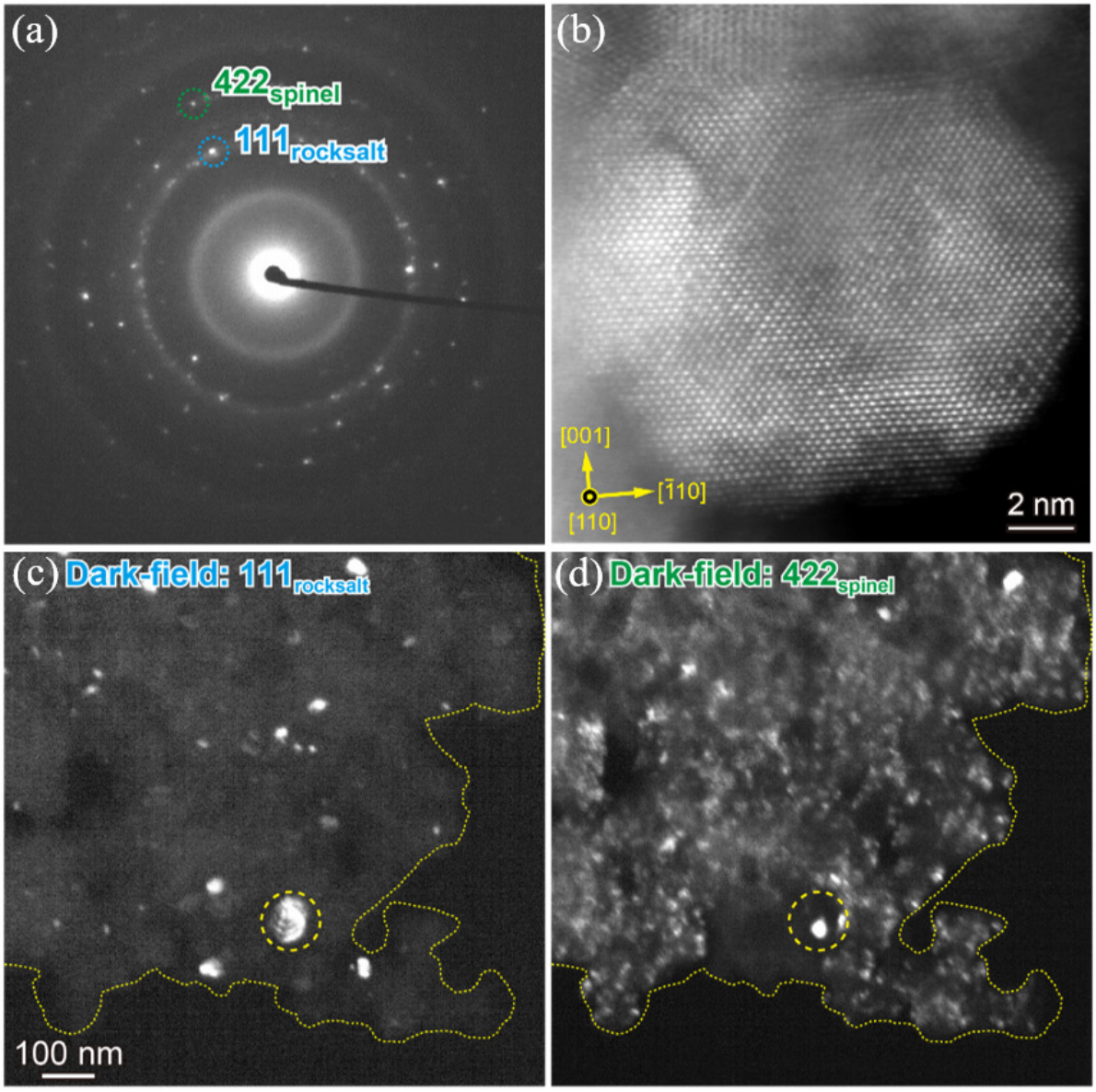

Figure S14: (a) Selected area diffraction pattern of $MgCo_2O_4$ powders after discharge. (b) HAADF-STEM image of a $MgCo_2O_4$ particle after discharge with core–shell (core: spinel, shell: rocksalt) structure. Dark field image obtained from (c) $111_{Rocksalt}$ and (d) 422_{Spinel} reflections, which also suggests the formation of core–shell structure.

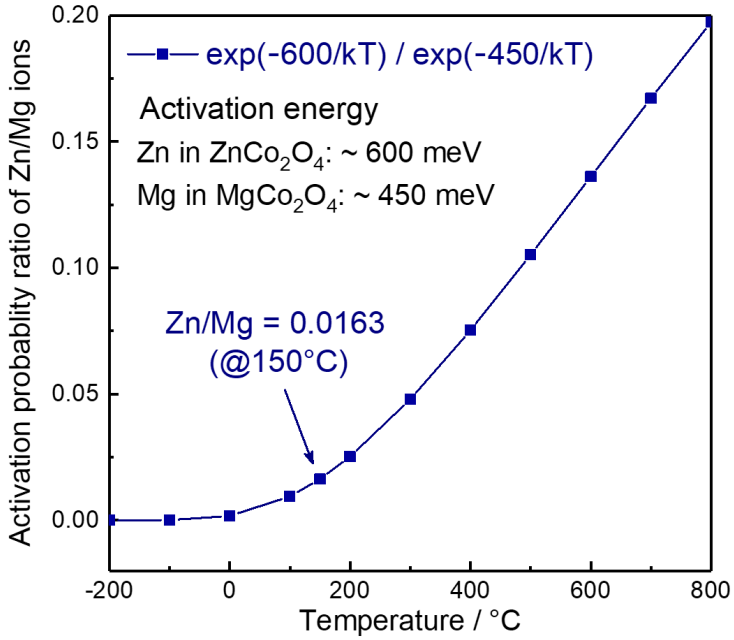

Figure S15: Activation probability ratio of Zn/Mg ions in spinel $(Zn/Mg)Co_2O_4$ host evaluated by the Boltzmann probability distribution. The activation energies for Zn and Mg are assumed to be 600 and 450 meV, respectively, based on the result of NEB calculation (Figure 2b in the main text).

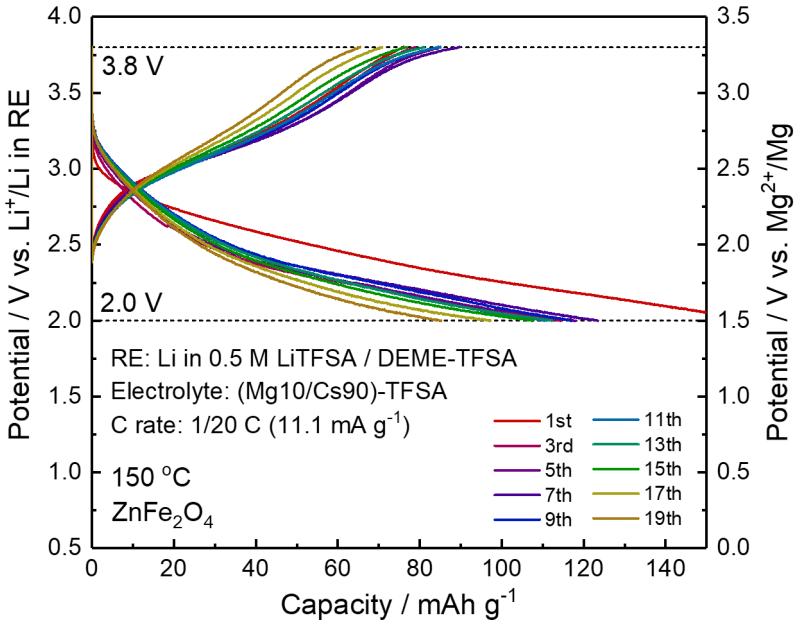

Figure S16: Galvanostatic discharge/charge performance of $ZnFe_2O_4$ in (Mg10/Cs90)TFSA at 1/20 C (11.1 mA g^{-1}) for 20 cycles. Capacity fading was observed after approximately 15 cycles.

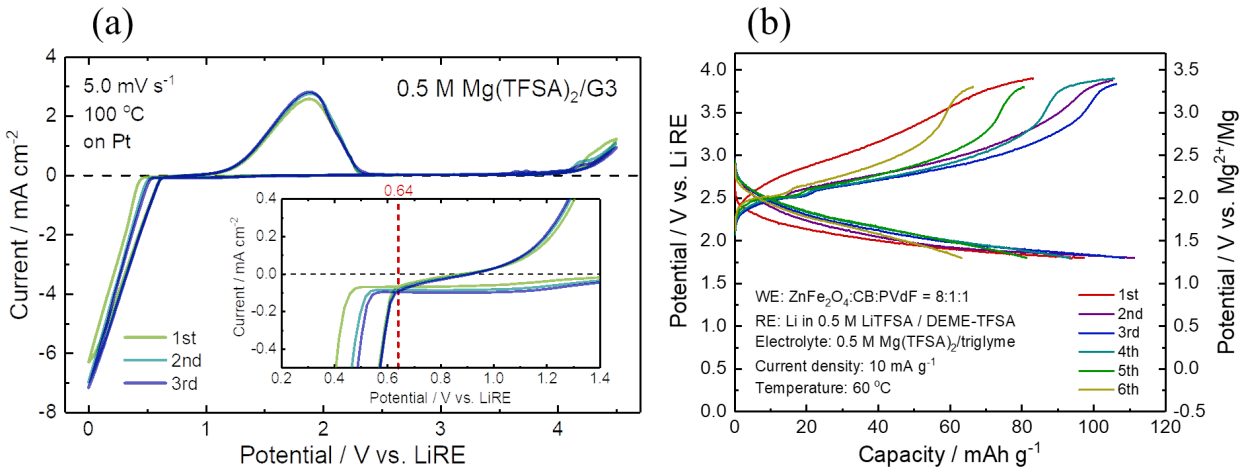

Figure S17: (a) Mg deposition/dissolution behavior in 0.5 M $Mg(TFSA)_2$/triglyme electrolyte at a scan rate of 5 mV s^{-1}. There observed a large overpotential of $\sim$ 1 V for Mg dissolution due to the passivation of deposited Mg. The redox potential of Mg^{2+}/Mg was determined to be approximately in the range of 0.6–0.8 V vs. LiRE considering the crossover points (inset). (b) Discharge/charge performance of $ZnFe_2O_4$ cathode for 6 cycles in a prototype cell with 0.5 M $Mg(TFSA)_2$/triglyme electrolyte at 60 °C.

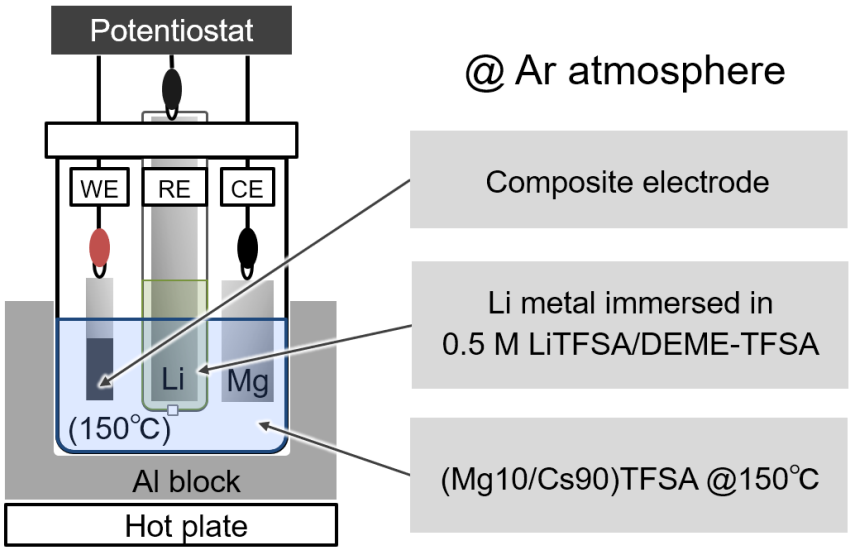

Figure S18: Schematic illustration of the three-electrode beaker-type cell used for electrochemical measurements. The beaker-type cell is heated by an aluminum block on a hot plate to maintain the electrolyte temperature at 150 °C.

References

(S1) Yagi, S.; Ichikawa, Y.; Yamada, I.; Doi, T.; Ichitsubo, T.; Matsubara, E. *Jpn. J. Appl. Phys.* **2013**, *52*, 025501.

(S2) Krezhov, K.; Konstantinov, P. *J. Phys.: Condens. Matter* **1993**, *5*, 9287–9294.

(S3) Fontaine, D. D. *Solid State Phys.* **1994**, *47*, 33–176.

(S4) Ceder, G.; der Ven, A. V.; Marianetti, C.; Morgan, D. *Modelling Simul. Mater. Sci. Eng.* **2000**, *8*, 311–321.

(S5) Morgan, D.; der Ven, A. V.; ; Ceder, G. *Electrochem. Solid-State Lett.* **2004**, *7*, A30–A32.

(S6) Ichitsubo, T.; Yagi, S.; Doi, T.; Yukitani, S.; Hirai, K.; Matsubara, E. *J. Electrochem. Soc.* **2012**, *159*, A14–A17.